doi.org/10.36721/PJPS.2026.39.2.REG.14913.1

Network pharmacology-based elucidation of the regulatory mechanism of *Solanum lyratum* (Bai Ying) against psoriasis via the IL-17A/STAT3 axis: Molecular docking and HaCaT cell validation

Zhaoxia Chen[1,2], Yonghao Zhang[1], Xuyang Han[3], Jianhua Qu[1]*, Tingting Di[3]* and Guangzhong Zhang[1]*

[1]Dermatological Department, Beijing Hospital of Traditional Chinese Medicine, Capital Medical University, Beijing 100010, China.
[2]Capital University of Economics and Business, Beijing 100070, China.
[3]Beijing Institute of Traditional Chinese Medicine, Beijing Hospital of Traditional Chinese Medicine, Capital Medical University, Beijing 100010, China.

Abstract: **Background**: Psoriasis affects approximately 2% of the global population, with the IL-17A-STAT3 pathway mediating abnormal keratinocyte proliferation and inflammatory amplification. Solanum lyratum (Bai Ying) has long been used for skin disorders, and its steroidal alkaloids have anti-inflammatory potential, though the mechanisms remain unclear. **Objective**: To elucidate the molecular basis and cytological efficacy of S. lyratum steroidal alkaloids in exerting anti-psoriatic effects via the IL-17A/STAT3 axis. **Methods**: HPLC-MS-QTOF, network pharmacology, molecular simulation, and a HaCaT cell model with STAT3-siRNA assays were employed. **Results**: Eighteen components were identified; steroidal alkaloids showed high affinity for STAT3 and IL17RA. S. lyratum (5–40 μg/mL) enhanced cell viability, inhibited p-STAT3 (IC50 = 14.30 μg/mL), and attenuated inflammatory responses and keratinocyte proliferation. **Conclusion**: S. lyratum steroidal alkaloids exert dual-targeted blocking effects on the IL-17A/STAT3 axis, supporting it as a potential therapeutic candidate for psoriasis.

Keywords: IL-17A/STAT3; Network pharmacology; Psoriasis; *Solanum lyratum*

Submitted on 26-07-2025 – Revised on 17-09-2025 – Accepted on 26-09-2025

INTRODUCTION

Psoriasis is an immune-mediated dermatosis characterized by chronic relapse and affecting approximately 2 % of the global population. The IL-23/IL-17A-Th17 axis is recognized as the core pathway driving abnormal keratinocyte proliferation and inflammation (Zhou *et al*., 2022). Although IL-17A or IL-17RA monoclonal antibodies and JAK-STAT inhibitors can significantly improve patient remission rates, their long-term use is limited by high cost, poor injection compliance, and the risk of immunosuppression-related infections (Guo *et al*., 2023). *Solanum lyratum* (Bai Ying, *S. lyratum*), a traditional heat-clearing and detoxifying herb, has been used in folk medicine for cutaneous inflammation and modern pharmacology has verified that its steroidal alkaloids possess anti-inflammatory, antioxidant and immunomodulatory activities (Zhao *et al*., 2022; Liu *et al*., 2023), however systematic elucidation of its psoriasis target spectrum and molecular mechanisms is still insufficient.

After activation, the IL-17A receptor complex converges on STAT3 phosphorylation and induces an amplification loop of inflammatory factors such as IL-6 and S100A9; blocking IL-17A signal input and STAT3 output is regarded as a promising strategy to disrupt the inflammation-proliferation cycle of psoriasis (Lee *et al*., 2024). In recent years, inhibitors targeting STAT3 and IL-17 have been developed and applied at a rapid pace. The novel STAT3-selective small-molecule inhibitor YY201 simultaneously inhibits the bifunctional phosphorylation of STAT3 and is over 1,000 times more active than other STAT3 small-molecule inhibitors currently in clinical trials. Currently, Phase I clinical studies are being conducted simultaneously in China and the United States (Chen *et al*., 2024). IL-17 inhibitors inhibit the activation of inflammatory signaling pathways and the development of diseases by specifically binding to the IL-17A cytokine in serum, blocking the binding of IL-17A to IL-17RA. Clinical studies have shown that up to 76.8% of patients can experience a more than 90% reduction in lesion size after two weeks of treatment with IL-17 inhibitors, offering new hope to patients with psoriasis (Kim *et al*., 2025).

The present study focuses on the inhibitory potential of steroidal alkaloids from *S. lyratum* targeting the dual nodes IL-17A/STAT3 and explores the feasibility of multi-target intervention by integrating network pharmacology, molecular docking and cellular validation. Current studies report that total saponins of *S. lyratum* alleviate mouse ear swelling and cellular oxidative stress (Yang *et al*., 2024), but how the core active constituents modulate the IL-17A pathway remains unclear; network pharmacology largely

**Corresponding authors:* e-mail: czx2006832@163.com; qujianhua@bjzhongyi.com; ditingting@bjzhongyi.com
*All corresponding authors have contributed equally to this work

remains computational and lacks a dynamics-plus-function experimental loop (Xiao *et al*., 2024); drug discovery on the IL-17A/STAT3 axis is still dominated by single-target strategies (Furtunescu *et al*., 2024), failing to simultaneously block the ligand-receptor interface and STAT3 transcriptional signaling. Moreover, in vitro models typically assess IL-17A-driven proliferation under serum-containing conditions (Yuan and Cao, 2023). However, these conditions do not replicate the context of nutrient deprivation and cytokine drive in lesions, which reduces the ability to detect the cytoprotective effects of natural products. In view of these gaps, this study established a serum-free (nutrient deprivation) + IL-17A dual-stimulation model, systematically maps the *S. lyratum* compound–target–pathway network, dissects the binding modes and energetic contributions of solanine-series steroidal alkaloids to STAT3 and IL-17RA, verifies their anti-inflammatory and anti-proliferative activities using p-STAT3, inflammatory mediators and cell-cycle indices and differentiates STAT3-independent components of the response via STAT3-siRNA, thereby providing integrated evidence for multi-target co-inhibition by *S. lyratum*. Using a closed-loop strategy spanning network pharmacology, molecular docking/dynamics, STAT3-siRNA and HaCaT functional assays, we show that *S. lyratum* steroidal alkaloids achieve synergistic anti-inflammatory effects by bidirectionally blocking the IL-17A receptor interface and STAT3 phosphorylation. Collectively, these findings clarify the inhibitory action of *S. lyratum* on IL-17-driven inflammatory activation in a serum-free (nutrient deprivation) context and provide experimental and structural support for developing potentially low-toxicity, orally available multi-target agents for psoriasis.

MATERIALS AND METHODS

Main reagents and materials

The main reagents and materials used in the experiments are listed in table 1.

Preparation of S. lyratum extract and quantification of chemical constituents

S. lyratum was pulverized and passed through a 60-mesh sieve. A total of 300 g of powder was reflux-extracted with 80 % ethanol (material: solvent = 1 g: 15 mL) for 2 h. The filtrate was rotary-evaporated under -0.08 MPa to a relative density of 1.10 (60ºC) and then freeze-dried at -50ºC for 48 h to obtain 37.8 g of light-brown total extract. To assess extraction-process reproducibility, three independent raw-herb batches (each 300 g) were processed with the identical protocol; extraction yield (%) was defined as (mass of freeze-dried extract / mass of raw powder) × 100, summarized as mean ± SD and the relative standard deviation (RSD) calculated as 100 × SD / mean. An aliquot of 10.00 mg of dried powder was ultrasonically dissolved in 10.00 mL of methanol (250 W, 40 kHz, 15 min) and filtered through a 0.22 μm PVDF membrane. HPLC-MS-QTOF analysis was performed on an XBridge C18 column (2.1 mm × 100 mm, 3.5 μm) at a flow rate of 0.3 mL·min^{-1} and a column temperature of 40ºC. Mobile phase A was 0.1 % formic acid-water and mobile phase B was 0.1 % formic acid-acetonitrile; gradient 0–15 min 5 %→95 %B. ESI positive-ion mode: spray voltage 3 500 V, drying gas 10 L·min^{-1}, nebulizer gas 45 psi, ion-source temperature 325ºC. Six-point external calibration curves (0.2–10 μg·mL^{-1}, r^2 > 0.999) were established for reference standards solanine and solasonine. The contents in the total extract were calculated as solanine 1.82 ± 0.07 mg·g^{-1} and solasonine 0.94 ± 0.04 mg·g^{-1}, reported as cross-batch means ± SD (n = 3) and the overall extraction yield across batches was 12.6 ± 0.3 % (n = 3; RSD = 2.4 %).

Network pharmacology analysis

Identification of active compounds and target prediction

Based on HPLC-MS identification, 18 structurally defined compounds were confirmed: solanine, solasonine, solamargine, chaconine, solasodine, tomatidine, β-sitosterol, diosgenin, chlorogenic acid, caffeic acid, ferulic acid, rutin, quercetin, kaempferol, hyperoside, astragalin, apigenin and luteolin. The canonical SMILES of each compound were downloaded and input separately into TCMSP, SwissTarget Prediction and PharmMapper. TCMSP parameters: Oral Bioavailability ≥ 30 %, Drug-Likeness ≥ 0.18; SwissTarget Prediction parameter: Probability ≥ 0.4; PharmMapper: top 300 NormFitScore. Targets obtained from the three databases were merged and de-duplicated to 428, then standardized to gene names using the UniProt "Homo sapiens" database.

Integration of psoriasis-related gene sets

A total of 352 "Psoriasis"-theme genes were downloaded from DisGeNET (v7.0). These were united with 367 genes whose "Psoriasis" scores in GeneCards were ≥ 20 and further combined with 153 differentially expressed genes ($|\log_2 FC| \geq 1.0$, FDR < 0.05) screened from the GEO-GSE14905 microarray dataset. After deduplication, 589 psoriasis-related genes were obtained.

KEGG/GO enrichment analysis and network construction

Metascape was used to perform GO-BP, GO-MF, GO-CC and KEGG analyses on 76 intersecting targets with the parameters: minimum gene count 3 and $p < 0.01$, followed by Benjamini-Hochberg correction. The results were imported into Cytoscape 3.10.2 and a drug-disease-target network was constructed according to Degree values, with STAT3 (Degree 37), IL17RA (Degree 33) and JAK2 (Degree 29) as the core nodes.

Molecular docking and molecular dynamics

Preparation of receptor and ligand structures

The IL-17A/IL-17RA complex (PDB 4HSA, resolution 2.50 A), STAT3 SH2 domain (PDB 6NUQ, 2.10 A) and JAK2 kinase domain (PDB 4IVA, 1.50 Å) were downloaded. The Schrödinger Protein Preparation Wizard was used to remove all ligands, ions and water molecules,

complete missing side chains and add hydrogen atoms; hydrogen-bond networks were optimized with PROPKA at pH 7.4. LigPrep generated 32 conformations for the 18 ligands using the OPLS4 force field, with ionization states automatically adjusted at pH 7.4 ± 0.5.

Molecular docking

Glide SP mode was used. The grid center for the IL-17RA interface was set at chain A Leu32 Cα (coordinates 7.2, 24.5, -8.3 A) with a cubic box edge length of 25 A; the grid center for the STAT3 Tyr705 region was set at chain A Lys591 Cα (-7.4, 14.2, 9.6 Å) with an edge length of 20 Å; the grid center for the JAK2 ATP pocket was set at chain A Lys882 Nζ (19.5, 3.7, 27.1 A) with an edge length of 18 Å. The top 20 conformations were retained and ranked according to GlideScore. Docking free energy showed that the solanine-STAT3 complex scored -8.43 kcal·mol^{-1}, comparable to the reference inhibitor Stattic at -8.57 kcal·mol^{-1}.

Molecular dynamics simulation

The three lowest-energy complexes (solanine-STAT3, solanine-IL-17RA and solasonine-STAT3) were simulated using AMBER 20. "tleap" loaded the ff14SB and GAFF force fields and a TIP3P water box was added with a 10 Å margin around each complex; Na^+ and Cl^- ions were added to a concentration of 0.15 mol·L^{-1}. Two-stage energy minimization was performed: first, with a 10 kcal·mol^{-1}·A^{-2} restraint on the backbone for 5 000 steps, then without restraint for another 5 000 steps. Subsequently, an NVT ensemble was used to heat the system to 300 K (50 ps), followed by NPT equilibration for 1 ns; the production run was 100 ns with a 2 fs timestep and SHAKE was applied to constrain bonds involving hydrogen. CPPTRAJ was used to calculate RMSD and H-bond occupancy and MMPBSA.py was used to calculate ΔG_bind. The solanine-STAT3 complex showed an average RMSD of 1.48 Å and a ΔG_bind of -57.2 kcal·mol^{-1}.

HaCaT cell validation

Cell culture and model establishment

HaCaT cells were cultured in DMEM high-glucose medium (10 % FBS, 100 U·mL^{-1} penicillin, 100 μg·mL^{-1} streptomycin) at 37°C in 5 % CO_2. When the cell index reached 0.8 × 10^6 cells cm^{-2}, the medium was replaced with serum-free DMEM for synchronization for 12 h (Zhou *et al*., 2023). Cells were then seeded in 6-well plates (growth area per well 9.6 cm²) at 2 × 10^5 cells·mL^{-1} in 2 mL. The model control group was stimulated with IL-17A at a final concentration of 100 ng·mL^{-1} for 24 h (Veras *et al*., 2022); experimental groups were simultaneously treated with *S. lyratum* total extract at 5, 10, 20 and 40 μg·mL^{-1}; the positive control group received Stattic 10 μM. Each group had independent wells n = 6, with three independent repetitions.

Cell viability and cytotoxicity

After 24 h treatment, 10 μL of CCK-8 solution was added to each well and incubated at 37°C for 1 h; absorbance was measured at 450 nm. Cell survival rate was calculated as (A_sample - A_blank)/(A_control - A_blank) × 100 %. The same batch of supernatant was assayed with an LDH activity kit (Jiancheng C0016) to assess membrane integrity and OD450 was converted to U·L^{-1} activity.

Detection of STAT3 Tyr705 phosphorylation

Cells were collected and washed three times with cold PBS, then lysed on ice for 30 min in 50 μL RIPA buffer containing 1 mM PMSF, 1 mM Na_3VO_4 and 1 mM NaF. Lysates were centrifuged at 12 000 g for 10 min and protein concentration was determined by the BCA method. For each sample, 30 μg of protein was separated on 10 % SDS-PAGE and transferred to a 0.45 μm PVDF membrane at a constant current of 300 mA for 90 min. Membranes were blocked with 5 % skim milk for 1 h, then incubated overnight at 4 °C with primary antibodies (p-STAT3 1:1000, STAT3 1:1000). After washing with PBS-T at room temperature for 3 × 10 min, membranes were incubated with secondary antibody 1:5000 at room temperature for 1 h. Chemiluminescence signals were captured using a ChemiDoc MP imaging system and band intensity was quantified with ImageJ. Inhibition rate was calculated as the ratio p-STAT3/STAT3 and IC_{50} was fitted with GraphPad Prism.

Inflammatory factor qPCR and ELISA

Total RNA was extracted using TRIzol and RNA purity was determined with a NanoDrop 2000; an A_{260}/A_{280} ratio of 1.8-2.0 was considered acceptable. The reverse-transcription system (total volume 20 μL) contained gDNA Remover 2 μL, RT buffer 4 μL, PrimeScript RT Enzyme Mix 1 μL, template RNA 1 μg and RNase-free water to 20 μL. The quantitative fluorescence PCR (qPCR) reaction system (total volume 20 μL) comprised TB Green Mix 10 μL, forward and reverse primers (10 μM) 0.4 μL each, cDNA template 2 μL and ddH_2O 7.2 μL. PCR cycling conditions were: 95°C pre-denaturation for 30 s; 95°C denaturation for 5 s and 60 °C annealing/extension for 30 s, for 40 cycles; after amplification, a 65-95 °C melting-curve analysis was performed to ensure product specificity. Relative gene expression was calculated by the 2^{-}ΔΔCt method, with GAPDH as the internal control. Primer sequences are shown in table 2.

Proliferation markers and cell-cycle detection

Immunofluorescence: After PBS washing, cells were fixed in 4 % paraformaldehyde for 20 min and permeabilized with 0.2 % Triton X-100 for 10 min, followed by blocking with 5 % BSA for 30 min. Primary antibodies Ki-67 (1:200) and Cyclin D1 (1:200) were added and incubated at 4 °C for 12 h. After three PBS-T washes, Alexa Fluor® 488 or 594 secondary antibody (1:500) was applied at room temperature for 1 h and nuclei were counterstained with DAPI 1 μg·mL^{-1} for 5 min. Five random fields were imaged under identical exposure settings using a Leica DMi8 confocal microscope and ImageJ was used to calculate the percentage of positive cells.

Cell cycle

Cells were fixed overnight at -20ºC in 70% ethanol, washed once with PBS and stained in 0.5 mL PI-RNase A working solution (50 μg·mL^{-1} PI, 100 μg·mL^{-1} RNase A) for 30 min at 37ºC in the dark. A BD FACSCalibur flow cytometer was used to collect 1 × 10^4 events and ModFit LT 5.0 calculated the proportions of G0/G1, S and G2/M phases.

STAT3 siRNA intervention

HaCaT cells were seeded in 6-well plates at 1 × 10^5 cells and incubated for 24 h. siRNA and Lipofectamine 3000 were diluted in Opti-MEM (final siRNA 50 nM, reagent 1.5 μL) and complexed at room temperature for 15 min before addition to the cells. After 6 h, the medium was replaced with complete medium and incubation continued for 24 h. According to the procedure in 2.5.1, cells were then co-treated with IL-17A and *S. lyratum* 20 μg·mL^{-1} for 24 h, followed by detection of p-STAT3 and inflammatory factors. Differences among the vector control, siRNA and siRNA + *S. lyratum* groups were compared.

Statistical analysis

All data were entered into GraphPad Prism 10.1. Normality was assessed with the Shapiro-Wilk test and homogeneity of variance with the Levene-Brown-Forsythe test. Data that met normality and homogeneity assumptions were analyzed by one-way ANOVA with Tukey post hoc test; when two factors were involved, two-way ANOVA with Sidak multiple-comparison correction was used. For comparisons between two groups, two-tailed independent-sample Student's t test was applied. Non-normal or heteroscedastic data were analyzed by Kruskal-Wallis test with Dunn correction. Dose-response curves and IC_{50} values were fitted using four-parameter nonlinear regression, with 95 % confidence intervals provided. For network pharmacology KEGG enrichment, multiple testing was corrected using the Benjamini-Hochberg method. Results are presented as mean ± SD or original data representing one of at least three independent experiments and two-sided $P < 0.05$ was considered statistically significant.

RESULTS

Identification and quantification of chemical constituents

Eighteen compounds were definitively identified in the ethanol extract of *S. lyratum* by HPLC-MS-QTOF. Steroidal alkaloids (solanine, solamargine, solasonine) showed higher contents of 1.82 ± 0.07, 1.05 ± 0.05 and 0.94 ± 0.04 mg·g^{-1}, respectively, whereas flavonoids and phenolic acids were relatively lower (Table 3). The HPLC-MS chromatogram exhibited 18 prominent peaks, with those corresponding to steroidal alkaloids showing significantly greater peak areas than other components, indicating that steroidal alkaloids are the dominant active constituents of *S. lyratum* (Fig. 1).

Network pharmacology prediction

Network topology analysis showed that the core anti-psoriatic targets of *S. lyratum* were centered on STAT3 (Degree = 37), IL17RA (Degree = 33) and JAK2 (Degree = 29), all possessing high betweenness centrality and closeness centrality, indicating that the IL-17A/STAT3 axis is the key pathway by which *S. lyratum* treats psoriasis (Table 4). KEGG enrichment, following hypergeometric testing and Benjamini-Hochberg correction, revealed significant clustering of overlapping targets in the IL-17 signaling pathway, Th17 cell differentiation, and the Jak-STAT pathway (all $P < 0.001$), suggesting that the anti-psoriatic effect of *S. lyratum* may involve modulation of IL-17/STAT3-related inflammatory and immune pathways (Fig. 2A). Network construction demonstrated that the active constituents of *S. lyratum* were closely connected to psoriasis-specific genes through key targets such as STAT3, IL17RA and JAK2, forming a distinct "drug–target–disease" interaction pattern and underscoring the central role of the IL-17A/STAT3 axis in the anti-psoriatic action of *S. lyratum* (Fig. 2B).

Molecular docking and molecular dynamics

Molecular docking showed that the GlideScore values of solanine, solasonine and solamargine toward STAT3 ranged from −8.02 to −8.43 kcal·mol^{-1}, close to that of the positive inhibitor Stattic-STAT3 (−8.57 kcal·mol^{-1}); key hydrogen bonds involved Lys591 and Arg595. For IL-17RA, solanine (−9.11) and solasonine (−8.65) exhibited stronger affinities, forming hydrogen bonds with Tyr56-OH and Asp107-OD1, respectively (Table 5). Molecular dynamics simulations revealed that the backbone RMSD values of the three ligand-target complexes reached dynamic equilibrium at approximately 60 ns (about 1.4–1.6 Å), with solanine-STAT3 showing the lowest fluctuation; hydrogen-bond analysis indicated that the critical hydrogen bond occupancy of the solanine-STAT3 complex was the highest and most stable (Fig. 3A,B). MM/GBSA analysis indicated that the binding free energies of solanine with STAT3 and IL17RA were −57.20 ± 1.85 and −61.55 ± 2.03 kcal·mol^{-1}, respectively; energy decomposition showed that hydrophobic interactions (ΔE_vdW and ΔG_nonpolar) contributed the most, suggesting that steroidal alkaloids bind stably to the targets of *S. lyratum* (Table 6).

Cellular functional validation

Treatment with *S. lyratum* at all tested concentrations significantly affected IL-17A-induced HaCaT cell viability and LDH release (One-way ANOVA, all $P < 0.001$). Tukey post-hoc tests further showed that, compared with the model group (0 μg·mL^{-1}), *S. lyratum* at 5–40 μg·mL^{-1} markedly increased HaCaT cell viability (all $P < 0.05$) while significantly decreasing extracellular LDH activity (all $P < 0.05$), indicating a clear dose-dependent cytoprotective effect against IL-17A-induced keratinocyte injury (Fig. 4A).

Table 1: List of main reagents and materials

Name	Source	Remarks
Solanum lyratum dried whole herb	IMPLAD herbarium, institute of medicinal plant development, chinese academy of medical sciences	
Solanine	Biopurify (Chengdu PuriPharm Technology Co., Ltd.)	Purity ≥ 98 %, confirmed by HPLC-UV
Solasonine	Biopurify (Chengdu PuriPharm Technology Co., Ltd.)	Purity ≥ 98 %, confirmed by HPLC-UV
Recombinant human IL-17A protein	PeproTech	Freshly prepared stock solution in 0.1 % BSA-PBS on the day of use
Anti-STAT3 (total protein)	Cell signaling technology	
Anti-p-STAT3 Tyr705	Cell signaling technology	
Anti-Ki-67	Cell signaling technology	
Anti-Cyclin D1	Cell signaling technology	
HRP-conjugated goat anti-rabbit IgG	Cell signaling technology	
HaCaT cell line	German DKFZ cell bank	Used after STR and mycoplasma negative testing
TRIzol™ reagent	Takara	
PrimeScript™ RT kit	Takara	
TB Green® Premix Ex Taq™ II	Takara	
Human IL-6 ELISA kit	R&D systems	
Human CXCL1 ELISA kit	R&D systems	
Human S100A9 ELISA kit	R&D systems	
Lipofectamine™ 3000	Thermo fisher scientific	
STAT3-siRNA	Thermo fisher scientific	Sense 5'-GCAAAUCUACAGCAUCUAU-3' Antisense 5'-AUAGAUGCUGUAGAUUUGC-3'
HPLC-MS-QTOF system	Agilent	
Ultrapure water system	Milli-Q	
Molecular simulation workstation	Intel Xeon Gold 6348	

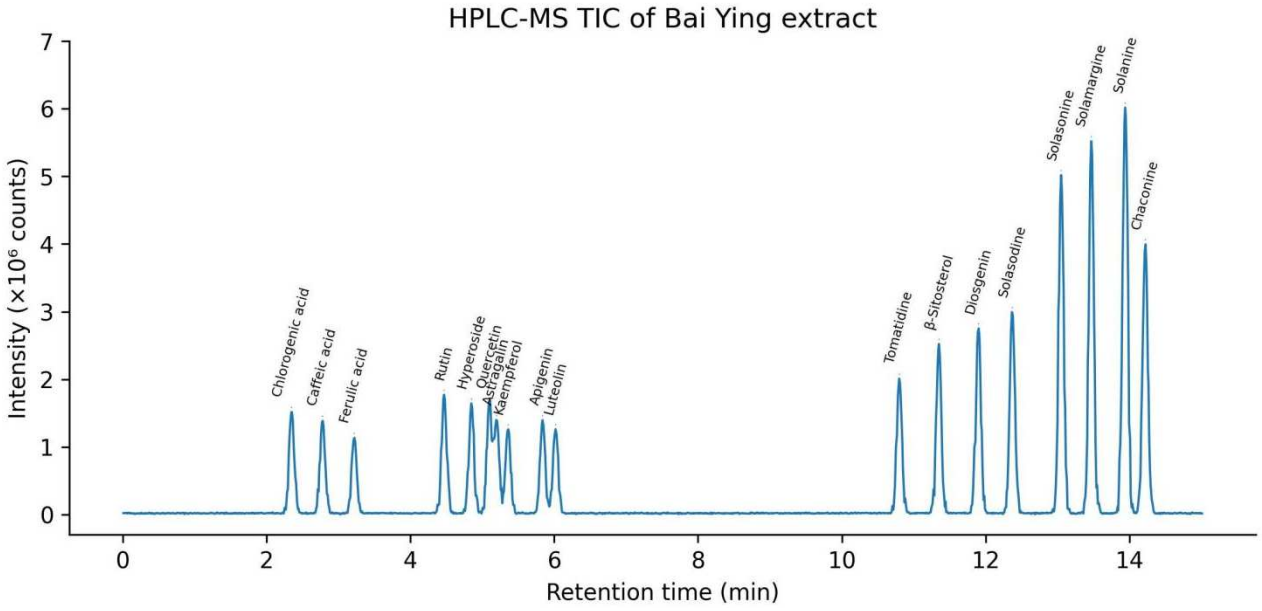

Fig. 1: HPLC-MS total ion chromatogram (TIC)

Table 2: Primer sequences

Target gene	Primer direction	Sequence (5' → 3')
IL-6	Forward	ACTCACCTCTTCAGAACGAATTG
	Reverse	CCATCTTTGGAAGGTTCAGGTTG
CXCL1	Forward	GACTTCCAGGCGAGGACACC
	Reverse	TGGGGACACCTTTTAGCATCTT
S100A9	Forward	CTGCGAAGTGTGGAGAAGCTG
	Reverse	TCCAGGTCCTCCCAGTAGACA
GAPDH	Forward	AGCCACATCGCTCAGACAC
	Reverse	GCCCAATACGACCAAATCC

Cell culture supernatants were collected simultaneously, and the protein levels of IL-6, CXCL1, and S100A9 were measured using ELISA kits. Procedures strictly followed the kit instructions: Incubation at room temperature for 2 h, four washes, addition of TMB substrate for color development for 15 min, termination of the reaction with 2 M H_2SO_4, and absorbance measurement at 450 nm. Protein concentrations were calculated from the standard curve.

Table 3: Quantitative results of major constituents in S. Iyratum extract ($mg \cdot g^{-1}$)

Compound name	Retention time (min)	Molecular formula	$[M+H]^+$ m/z	Content ($\bar{x} \pm s$, $mg \cdot g^{-1}$)
Solanine	13.94	$C_{45}H_{73}NO_{15}$	868.51	1.82 ± 0.07
Solasonine	13.05	$C_{45}H_{73}NO_{16}$	884.50	0.94 ± 0.04
Solamargine	13.47	$C_{45}H_{73}NO_{15}$	868.51	1.05 ± 0.05
β-Sitosterol	11.35	$C_{29}H_{50}O$	415.39	0.31 ± 0.02
Diosgenin	11.90	$C_{27}H_{42}O_3$	415.32	0.26 ± 0.02
Chlorogenic acid	2.35	$C_{16}H_{18}O_9$	355.10	0.44 ± 0.03
Caffeic acid	2.78	$C_9H_8O_4$	181.05	0.37 ± 0.02
Ferulic acid	3.22	$C_{10}H_{10}O_4$	195.07	0.19 ± 0.01
Rutin	4.47	$C_{27}H_{30}O_{16}$	611.16	0.58 ± 0.04
Quercetin	5.10	$C_{15}H_{10}O_7$	303.05	0.43 ± 0.03
Kaempferol	5.36	$C_{15}H_{10}O_6$	287.06	0.29 ± 0.02
Hyperoside	4.85	$C_{21}H_{20}O_{12}$	465.10	0.24 ± 0.01
Astragalin	5.20	$C_{21}H_{20}O_{11}$	449.11	0.21 ± 0.01
Apigenin	5.84	$C_{15}H_{10}O_5$	271.06	0.27 ± 0.02
Luteolin	6.02	$C_{15}H_{10}O_6$	287.06	0.30 ± 0.02
Tomatidine	10.80	$C_{27}H_{45}NO_2$	416.35	0.22 ± 0.01
Chaconine	14.22	$C_{45}H_{73}NO_{14}$	852.51	0.68 ± 0.03
Solasodine	12.37	$C_{27}H_{43}NO_2$	414.34	0.18 ± 0.01

Note: Determination method was 80 % ethanol extraction-HPLC-MS-QTOF.

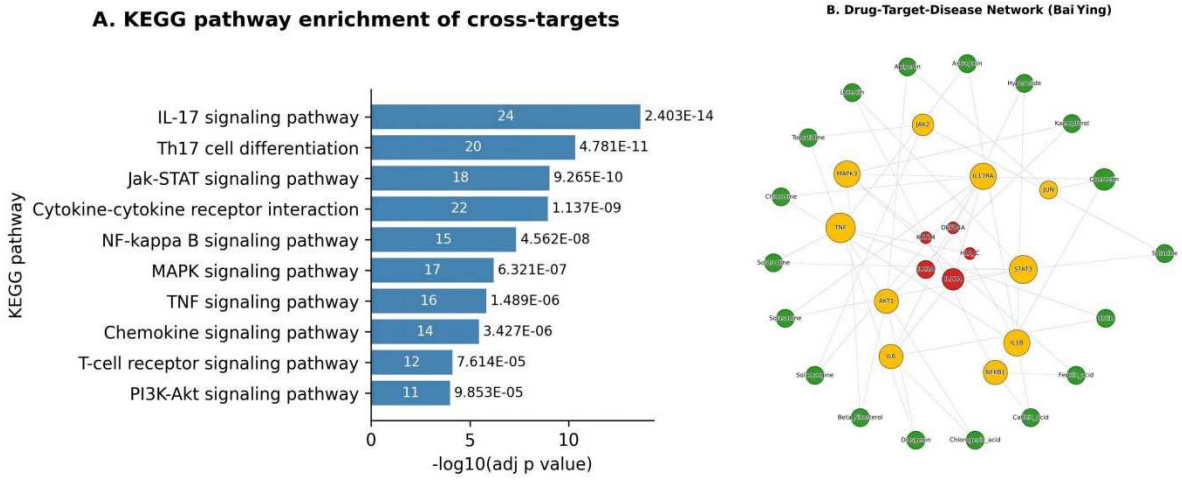

Fig. 2: Network pharmacology target screening and pathway enrichment analysis. A: KEGG enrichment bar chart of intersecting targets. B: Schematic diagram highlighting the central role of STAT3 and IL17RA.

Table 4: Topological parameters of core overlapping targets in the PPI network

Gene symbol	Degree	Betweenness centrality	Closeness centrality
STAT3	37	0.19	0.55
IL17RA	33	0.15	0.53
JAK2	29	0.14	0.52
MAPK3	25	0.13	0.51
TNF	24	0.12	0.49
AKT1	23	0.12	0.49
IL6	22	0.11	0.49
NFKB1	21	0.10	0.49
IL1B	19	0.10	0.48
JUN	18	0.09	0.48

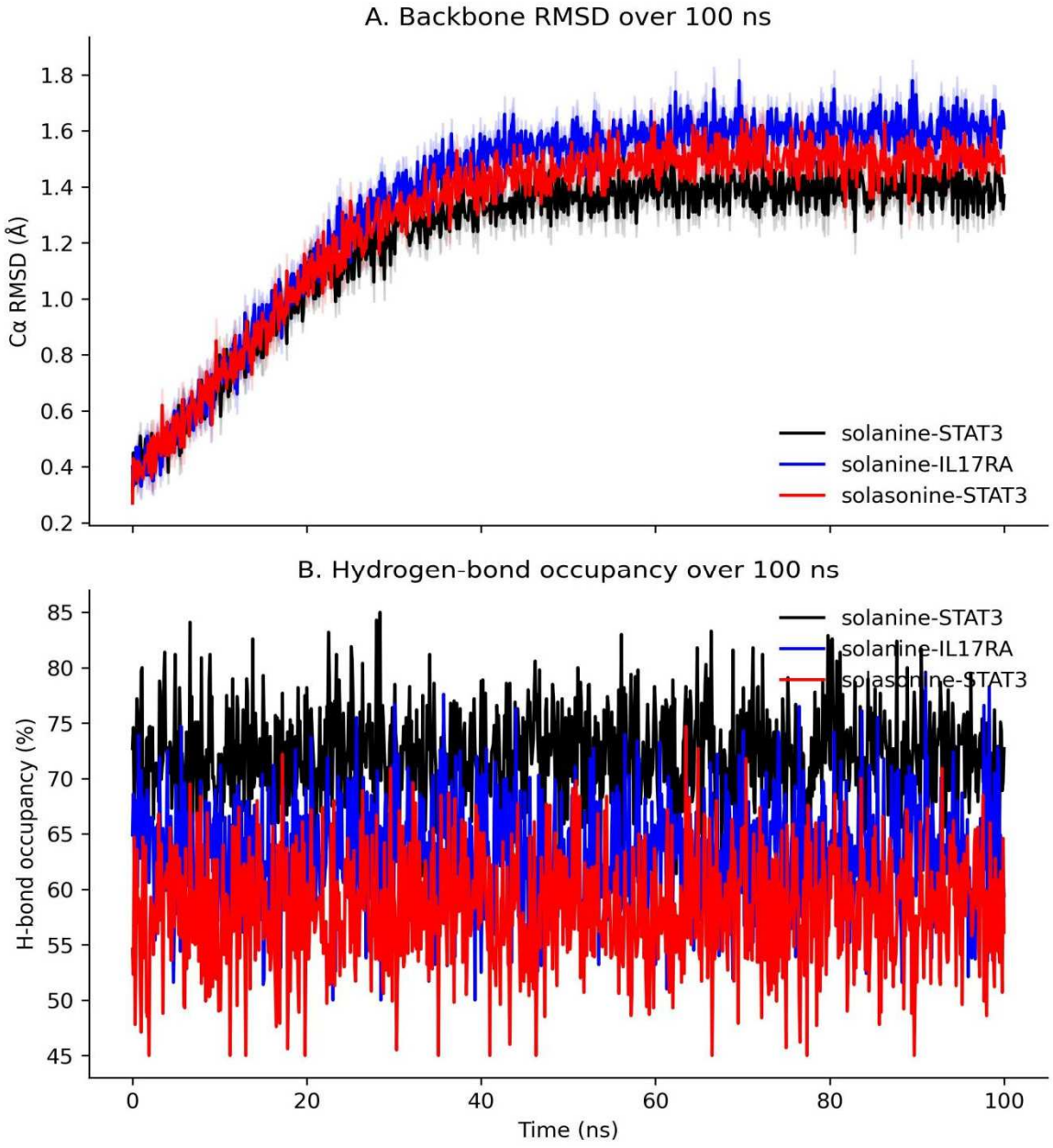

Fig. 3: 100 ns MD simulation metrics. A: Backbone RMSD (Å) of complexes, sampling step 0.1 ns; mean ± SD over the full trajectory. B: Hydrogen-bond occupancy (%).

Table 5: Glide docking scores and key hydrogen bonds of major compounds toward three targets

Compound	Target	GlideScore (kcal·mol^{-1})	Key hydrogen-bond residues	H-bond distance (A)
Solanine	STAT3	−8.43	Lys591-NZ···O(ligand)	2.14
Solanine	IL17RA	−9.11	Tyr56-OH···O(ligand)	2.71
Solanine	JAK2	−7.62	Lys882-NZ···O(ligand)	2.39
Solasonine	STAT3	−8.20	Arg595-NH2···O(ligand)	2.06
Solasonine	IL17RA	−8.65	Asp107-OD1···N(ligand)	2.84
Solasonine	JAK2	−7.40	Glu930-OE1···N(ligand)	2.27
Solamargine	STAT3	−8.02	Ser636-OG···O(ligand)	2.58
Stattic[2]	STAT3	−8.57	Lys591-NZ···O(ligand)	2.19

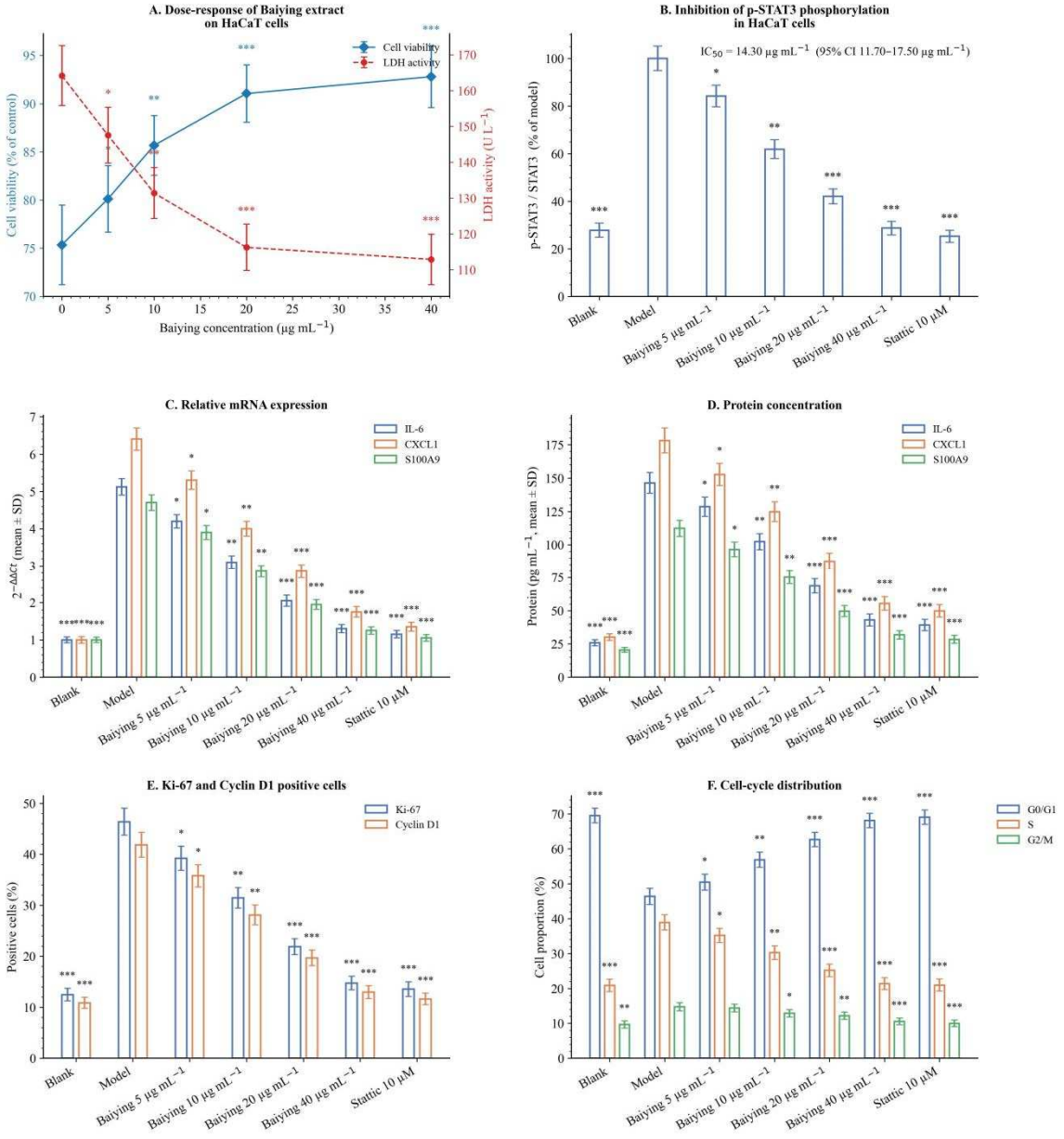

Fig. 4: S. Iyratum suppresses IL-17A-induced inflammation, STAT3 activation, and proliferation in HaCaT cells. A: Dose-response curves for HaCaT cell viability and LDH leakage. B: p-STAT3 Western blot and densitometric quantification. C: Relative mRNA expression. D: Protein concentration. E: Ki-67 and Cyclin D1 immunofluorescence. F: Cell-cycle analysis. Each group had independent wells n = 6, with three independent repetitions. Significance symbols: *P < 0.05, **P < 0.01, ***P < 0.001 vs corresponding model group.

Table 6: Summary of MM/GBSA binding free energies ($\bar{x} \pm s$, kcal·mol^{-1})

Complex	ΔG_bind	ΔE_vdW	ΔE_ele	ΔG_polar	ΔG_nonpolar
Solanine-STAT3	−57.20 ± 1.85	−44.37 ± 1.22	−24.62 ± 1.10	+21.18 ± 0.96	−9.39 ± 0.53
Solanine-IL17RA	−61.55 ± 2.03	−46.01 ± 1.35	−27.14 ± 1.28	+22.57 ± 1.04	−10.97 ± 0.61
Solasonine-STAT3	−54.78 ± 1.67	−42.89 ± 1.09	−22.33 ± 0.98	+20.47 ± 0.87	−10.03 ± 0.49
Stattic-STAT3	−58.03 ± 1.92	−45.66 ± 1.18	−23.85 ± 1.07	+20.12 ± 0.95	−8.64 ± 0.51

Note: Stattic serves as the positive control for STAT3 inhibition. Results were obtained from the last 20 ns (200 frames) of MM/GBSA calculations; more negative values indicate more stable binding.

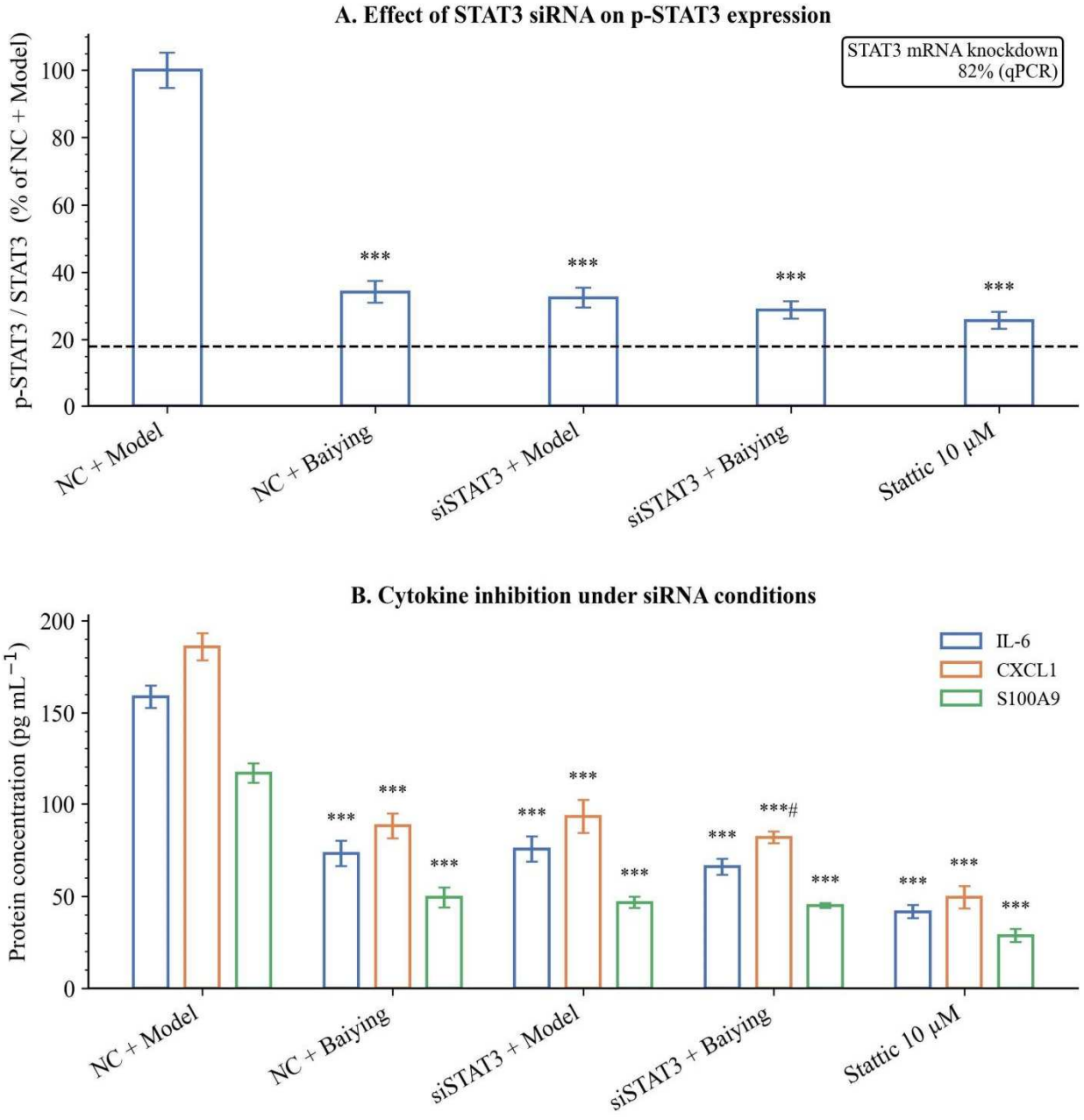

Fig. 5: STAT3-siRNA verification of the STAT3 dependence of the anti-inflammatory effect of S. Iyratum.
A: p-STAT3 expression after STAT3-siRNA knockdown. B: Comparison of inflammatory-factor inhibition under siRNA conditions. Each group had independent wells n = 6, with three independent repetitions. Significance symbols: *P < 0.05, **P < 0.01, ***P < 0.001 vs corresponding NC + model; #P < 0.05, ##P < 0.01, ###P < 0.001 siSTAT3 + S. lyratum vs siSTAT3 + model.

p-STAT3 expression in the *S. lyratum* treatment groups of different concentrations and in the positive-control group (Stattic 10 μM) was significantly lower than that in the model group (One-way ANOVA, $P < 0.001$). Tukey tests confirmed a dose-dependent inhibitory effect (all $P < 0.05$) and the positive-control group was also significantly lower than the model group ($P < 0.001$). The IC_{50} value obtained by four-parameter logistic regression was 14.30 $\mu g \cdot mL^{-1}$ (95 % CI 11.70–17.50 $\mu g \cdot mL^{-1}$) (Fig. 4B).

Significant differences were observed among groups in the mRNA expression levels and protein concentrations of IL-6, CXCL1 and S100A9 (One-way ANOVA, all $P < 0.001$). Tukey post-hoc tests indicated that all concentrations of *S. lyratum* and the positive control (Stattic 10 μM) significantly reduced IL-17A-induced IL-6, CXCL1 and S100A9 mRNA expression and protein levels in HaCaT cells (vs model group, all $P < 0.05$), with a pronounced dose-dependent inhibition (Figs. 4C, D).

The positive-cell rates of Ki-67 and Cyclin D1 differed significantly among groups (One-way ANOVA, all $P < 0.001$). Tukey tests showed that every *S. lyratum* concentration and the positive control significantly lowered IL-17A-induced Ki-67 and Cyclin D1 positivity in HaCaT cells (vs model group, all $P < 0.05$) in a dose-dependent manner (Fig. 4E).

Proportions of G0/G1, S and G2/M phases also differed significantly among groups (One-way ANOVA, all $P < 0.01$). Tukey tests demonstrated that each *S. lyratum* concentration and the positive control significantly increased the G0/G1 phase proportion and markedly decreased the S and G2/M phase proportions (vs model group, all $P < 0.05$), again displaying a clear dose-dependent trend (Fig. 4F).

STAT3 dependency verification

Significant differences in p-STAT3 expression were observed among the experimental groups (One-way ANOVA, $P < 0.001$); Tukey tests showed that p-STAT3 levels in all groups were markedly lower than those in the NC + model group (all $P < 0.001$), whereas no statistically significant difference was found between the siSTAT3 + *S. lyratum* and the siSTAT3 + model groups ($P > 0.05$) (Fig. 5A). Both siRNA and the drug exhibited significant main effects and interaction effects on the inhibition of IL-6, CXCL1 and S100A9 protein concentrations in HaCaT cells by *S. lyratum* (Two-way ANOVA, all $P < 0.001$); Sidak-corrected post-hoc tests indicated that protein levels in all treatment groups were significantly lower than those in the NC + model group (all $P < 0.001$). Only the CXCL1 protein level in the siSTAT3 + *S. lyratum* group was significantly lower than that in the siSTAT3 + model group ($P < 0.05$) and this trend was not observed for the other factors (Fig. 5B).

DISCUSSION

This study confirmed that the ethanol extract of *S. lyratum* is dominated by steroidal alkaloids, with solanine, solasonine and solamargine displaying markedly higher abundances and peak areas, thereby laying the chemical foundation for its pharmacological activity. Reverse pharmacophore-based target prediction intersected with psoriasis-related gene sets, identifying over 70 common targets, with STAT3, IL17RA, and JAK2 emerging as central nodes in the network topology. Pathway enrichment clustered these targets within the IL-17 and JAK-STAT signaling pathways, underscoring the strong mechanistic association between steroidal alkaloids and psoriasis pathogenesis. The molecular architecture of steroidal alkaloids, comprising a hydrophobic steroid nucleus and multiple hydroxylated sugar moieties, facilitates stable hydrogen bonding and hydrophobic interactions at both the IL-17A/IL17RA interface and within the STAT3 SH2 domain. This dual-target engagement effectively blocks upstream signal input and downstream transcriptional amplification, thereby suppressing inflammatory cascades, keratinocyte hyperproliferation, and immune crosstalk (Wu *et al*., 2024). Recent clinical studies have shown that Th17 immune imbalance mediated by IL-17A is the fundamental cause of psoriatic lesions; IL-17A monoclonal antibodies can rapidly improve plaques, but long-term injections and mucosal fungal infections limit compliance (Bilal *et al*., 2023). Although oral JAK inhibitors can down-regulate STAT phosphorylation, they are accompanied by safety risks such as thrombosis and viral reactivation (Winthrop and Cohen, 2022), so natural alternatives with good safety profiles attract considerable clinical interest. The binding free energy of *S. lyratum* steroidal alkaloids to STAT3 is comparable to that of classic inhibitors, while their affinity for IL17RA is even higher(Sahu *et al*., 2023), presenting a natural integrated regulatory advantage of “multi-target, low-toxicity” that better matches the cost and safety requirements for chronic management of psoriasis(Le *et al*., 2024). Moreover, their dose-dependent inhibitory effect provides a clear dose-response reference for subsequent clinical development and offers a reliable structural template and pharmacodynamic basis for targeted optimization of the steroidal alkaloid scaffold.

The results of molecular docking and dynamics demonstrated that the solanine-series steroidal alkaloids exhibit sub-micromolar affinity at both the STAT3 SH2 pocket and the IL17RA-chain A interface; the complex RMSD remained on a 1.4-1.6 A plateau with >60 % hydrogen-bond occupancy throughout the trajectory, confirming stable binding. Binding free-energy decomposition indicated that ΔE_vdW and ΔG_nonpolar were the main contributors (Forouzesh and Mishra, 2021), consistent with steroid-aromatic stacking and hydrophobic sandwich conformations. Robust hydrogen bonds

involving key residues Lys591, Arg595, Tyr56 and Asp107 further reduced desolvation energy loss, spatially blocking both IL-17A ligand engagement and downstream STAT3 dimerization, thereby inactivating signal input and transcriptional output in two directions (Wang *et al*., 2025a). Notably, the binding free energy of the solanine-IL17RA complex was higher than that of the IL-17RA antagonistic peptides currently reported, while the solanine-STAT3 complex was only 0.13 kcal·mol^{-1} weaker than Stattic, indicating that a single molecule can exert dual functions of "ligand-receptor blockade" and "transcription-factor inhibition" simultaneously(Wang *et al*., 2025b). Many STAT3 small-molecule antagonists in clinical development have insufficient affinity or specificity; the steroidal alkaloid scaffold presented here meets three key pharmacodynamic criteria: high affinity, multi-target activity, and low polarity. This provides a credible structural starting point for directed modification based on the natural steroid nucleus. Combined with the cellular finding that *S. lyratum* yielded a p-STAT3 IC_{50} of 14.3 μg·mL^{-1}, paralleling the siSTAT3 effect, it can be inferred that direct binding of steroidal alkaloids is the decisive factor for inhibiting STAT3 phosphorylation at the cellular level. More importantly, dual targeting of IL17RA and STAT3 may reduce the risk of resistance mutations at a single site, offering a pharmacological advantage for long-term intervention in chronic recurrent psoriasis and laying an experimental foundation for an integrated "ligand-receptor-transcription factor" blockade strategy.

In the serum-free (nutrient deprivation) + IL-17A combined injury model, the total extract of *S. lyratum* dose-dependently increased HaCaT cell viability and reduced LDH leakage, suggesting that it can maintain energy metabolism and membrane integrity; the half-maximal inhibitory concentration of p-STAT3 was 14.3 μg·mL^{-1}, consistent with the high-affinity prediction from molecular dynamics, confirming that STAT3 inactivation is the principal mechanism. The transcription and protein levels of downstream inflammatory factors IL-6 and S100A9 were markedly attenuated and although CXCL1 also decreased, partial inhibition remained under STAT3 knockdown, indicating that *S. lyratum* may also exert compensatory regulation through STAT3-independent pathways (such as p38-MAPK) (Zheng *et al*., 2024). The positive rates of Ki-67 and Cyclin D1 declined with increasing concentrations of *S. lyratum* and the cell cycle shifted from S and G2/M phases back to the G0/G1 phase, demonstrating effective inhibition of the STAT3-Cyclin D1 axis and a transition of cells from pathological proliferation to quiescence (Peng *et al*., 2023). Compared with the simple IL-17A-induced proliferative system, this study used serum-free (nutrient deprivation) conditions to better approximate the lesional microenvironment of psoriasis. Under these conditions, the IL-17A-induced injury phenotype was observed and *S. lyratum* still significantly enhanced viability, reflecting anti-inflammatory and cytoprotective effects (Yao *et al*., 2024). STAT3-siRNA alone inhibited inflammation to a similar extent to S. lyratum, and there was no evidence of a synergistic effect when the two were combined. This suggests that *S. lyratum's* activity is indeed STAT3-dominated. The residual effect on CXCL1 indicates the presence of secondary targets, which is consistent with the higher degree of the p38-MAPK node predicted by network pharmacology (Jo *et al*., 2025). Clinically, IL-17A biologics rapidly clear plaques but are costly and lack direct cytoprotective activity, while small-molecule JAK/STAT inhibitors carry risks of thrombosis (Nyholm *et al*., 2023); *S. lyratum* maintains viability, inhibits STAT3, dampens the NF-κB-IL-6 amplification loop and normalizes the cell cycle, providing a potentially low-toxicity natural candidate suitable for long-term management of psoriasis and offering a mechanistic basis for combining steroidal alkaloids with biologics or antioxidants.

Limitations

This study elucidated the inhibitory action of *S. lyratum* steroidal alkaloids on the IL-17A/STAT3 axis through a "network pharmacology–molecular docking-cellular validation" strategy, yet several limitations remain. According to relevant literature, the in vitro drug observation concentration is 5-40μg·mL. In vitro exposure for 24 hours cannot directly infer the true pharmacokinetics in the lesion tissue. In addition, this study lacks in vivo research. Therefore, a pharmacokinetic–pharmacodynamic relationship for transdermal administration should be established in an imiquimod mouse model and the reparative effect of long-term application on psoriatic lesions should be evaluated. Molecular docking and dynamics simulations focused only on the binding of the solanine series to STAT3 and IL-17RA, without systematically analyzing other constituents or bypass nodes such as JAK2 and p38-MAPK; subsequent work should expand the docking library and verify multi-target synergy through key-residue mutation and surface plasmon resonance assays. HaCaT cells lack dermal-immune interaction and gene expression differs from patient-derived primary keratinocytes, so *S. lyratum* may have additional immunoregulatory effects; future studies should use IMQ-induced primary keratinocytes or 3D skin models to enhance clinical translatability. The STAT3-siRNA knockdown efficiency in this experiment reached 82 %, which verified the core role of STAT3, but residual expression might mask contributions from non-STAT3 targets; subsequent work can employ CRISPR-Cas9 to establish STAT3-knockout models and integrate multi-omics analyses to comprehensively dissect the signaling network and metabolic pathways of steroidal alkaloids. These measures will further clarify the effective exposure window and potential targets of *S. lyratum*, providing a firmer experimental basis for its preclinical development.

CONCLUSION

S. lyratum is rich in steroidal alkaloids and network pharmacology pinpointed the IL-17A/STAT3 axis as its core site of action; molecular docking, MD and MM/GBSA demonstrated that the solanine series shows high affinity and stable binding to both STAT3 and IL-17RA, with hydrophobic and hydrogen-bond interactions synergistically furnishing a dual-target blockade. In a HaCaT model simulating serum-free (nutrient deprivation) + IL-17A dual stimulation, *S. lyratum* dose-dependently enhanced cell viability, inhibited p-STAT3 and IL-6, CXCL1, S100A9 expression and restored cell-cycle quiescence; STAT3-siRNA verified that its anti-inflammatory and anti-proliferative effects primarily depend on STAT3 inactivation. Overall evidence indicates that *S. lyratum* attenuates the inflammatory amplification loop and confers cytoprotection to keratinocytes by bidirectionally targeting the IL-17A receptor interface and the STAT3 transcriptional axis, providing experimental support for developing potentially low-toxicity, orally available, multi-target candidates and for the long-term management of psoriasis.

Acknowledgement
This work was supported by the National Natural Science Foundation of China (82274523) and Beijing Municipal Hospitals' Research and Development Program (PZ2023020).

Author's contributions
Study concepts: Tingting Di, Jianhua Qu and Guangzhong Zhang
Study design: Zhaoxia Chen, Tingting Di and Guangzhong Zhang
Definition of intellectual content: Yonghao Zhang
Literature research: Zhaoxia Chen and Tingting Di
Clinical studies: Zhaoxia Chen, Yonghao Zhang, Jianhua Qu and Guangzhong Zhang
Experimental studies: Tingting Di and Xuyang Han
Data acquisition: Zhaoxia Chen, Yonghao Zhang, Tingting D and Xuyang Han
Data analysis: Zhaoxia Chen and Yonghao Zhang
Statistical analysis: Zhaoxia Chen and Tingting Di
Manuscript preparation: Zhaoxia Chen
Manuscript editing: Zhaoxia Chen, Yonghao Zhang and Xuyang Han
Manuscript review: Tingting Di, Jianhua Qu and Guangzhong Zhang

Funding
There was no funding.

Data availability statement
The datasets generated during and/or analysed during the current study are available from the corresponding author on reasonable request.

Ethical approval
Not applicable.

Conflict of interest
All the authors declare that there were no conflicts of interest.

REFERENCES

Bilal H, Khan MN, Khan S, Fang W, Chang W, Yin B and Liu Z (2023). Risk of candidiasis associated with interleukin-17 inhibitors: Implications and management. *Mycology*, **15**(1): 30-44.

Chen H, Bian A, Zhou W, Miao Y, Ye J, Li J, He P, Zhang Q, Sun Y, Sun Z, Ti C, Chen Y, Yi Z and Liu M (2024). Discovery of the highly selective and potent STAT3 inhibitor for pancreatic cancer treatment. *ACS Cent. Sci*., **10**(3): 579-594.

Forouzesh N and Mishra N (2021). An effective MM/GBSA protocol for absolute binding free-energy calculations: A case study on SARS-CoV-2 spike protein and the human ACE2 receptor. *Molecules*, **26**(8): 2383.

Furtunescu AR, Georgescu SR, Tampa M and Matei C (2024). Inhibition of the JAK-STAT pathway in the treatment of psoriasis: A review of the literature. *Int. J. Mol. Sci*., **25**(9): 4681.

Guo J, Zhang H, Lin W, Lu L, Su J and Chen X (2023). Signaling pathways and targeted therapies for psoriasis. *Signal Transduct. Target Ther*., **8**: 437.

Jo HG, Seo J, Jang B, Kim Y and Lee S (2025). Integrating network pharmacology and experimental validation to advance psoriasis treatment: Multi-target mechanistic elucidation of medicinal herbs and natural compounds. *Autoimmun. Rev*., **24**(186): 103836.

Kim D, Yang S, Gill M, Babaei N, Cervantes M and Wu JJ (2025). Next-generation anti-IL-17 agents for psoriatic disease: A pipeline review. *Am. J. Clin. Dermatol*., **26**(3): 307-320.

Le S, Wu X, Dou Y, Song T, Fu H, Luo H, Zhang F and Cao Y (2024). Promising strategies in natural products treatments of psoriasis-update. *Front. Med*., **11**: 1386783.

Lee YG, Jung Y, Choi HK, Lee JI, Lim TG and Lee J (2024). Natural product-derived compounds targeting keratinocytes and molecular pathways in psoriasis therapeutics. *Int. J. Mol. Sci*., **25**(11): 6068.

Liu X, Wang F, Chen Y, An Y, Cheng L, Wang L, Kong D, Zhao W, Tian J, Niu Y, Cui W, Zhang W, Xu Y, Ba Y, and Zhou HL (2023). Research progress on chemical components and pharmacological action of *Solanum lyratum* Thunb. *J. Pharm. Pharmacol.*, **75**(3): 328–362.

Nyholm N, Danø A, Schnack H and Colombo GL (2023). The cost-effectiveness of anti-IL-17 biologic therapies for moderate-to-severe plaque psoriasis treatment in Italy and Germany: A sequential treatment analysis. Clinicoecon. *Outcomes Res.,* **15**: 607–619.

Peng Y, Zhang Y, Luo M, Pan Y, Zhou R, Yan YN, Yi T,

Luo F, Wang B, Wang L, Ran C and Wang H (2023). NEK2 over-expression aggravates IL-22-induced keratinocyte proliferation, cytokine production and imiquimod-induced psoriasis-like dermatitis. *Biochim. Biophys. Acta Mol. Cell Res.,* **1870**(8): 119525.

Sahu N, Madan S, Walia R, Tyagi R, Fantoukh OI, Hawwal MF, Akhtar A, Almarabi I, Alam P and Saxena S (2023). Multi-target mechanism of *Solanum xanthocarpum* for treatment of psoriasis based on network pharmacology and molecular docking. *Saudi Pharm. J.* **31**(5): 101788.

Veras FP, Publio GA, Melo BM, Prado DS, Norbiato T, Cecilio NT, Hiroki C, Damasceno LEA, Jung R, Toller-Kawahisa JE, Martins TV, Assunção SF, Lima D, Alves MG, Vieira GV, Tavares LA, Alves-Rezende ALR, Karbach SH, Nakaya HI, Cunha TM, Souza CS, Cunha FQ, Sales KU, Waisman A and Alves-Filho JC (2022). Pyruvate kinase M2 mediates IL-17 signaling in keratinocytes driving psoriatic skin inflammation. *Cell Rep*., **41**(13): 111897.

Wang J, Zhang P, Yu Y, Yi Y, Jiang Y and Hu S (2025). Discovery of novel STAT3 inhibitors with anti-breast cancer activity: Structure-based virtual screening, molecular dynamics and biological evaluation. *RSC Med. Chem.,* (Advance online).

Wang X, Bao H, Wang Y, Wang Y, Guo C, Wu Y, Xu Y and Li Y (2025). Innovative peptide therapeutics targeting IL17RA to regulate inflammatory responses. *Sci Rep.,* **15**(1): 8542

Winthrop KL and Cohen SB (2022). Oral surveillance and JAK inhibitor safety: The theory of relativity. *Nat. Rev. Rheumatol,* **18**(5): 301–304.

Wu T, Du X, Liu HH, Liu LY, Yang YK, Wang SJ and Duan CL (2024). Bioactive solanidane steroidal alkaloids from *Solanum lyratum*. *Fitoterapia,* **175**: 105916.

Xiao H, Gui Y, Li X, Dai W and colleagues (2024). Explore on screening COX-2 inhibitors from the essential oil of *Solanum lyratum* Thunb. by molecular docking and molecular dynamics simulation. *Heliyon,* **10**(15): e37652.

Yang L, Yang Y, Wang Q, Fei H, Fei R, Xu Y and Zhang C (2024). Anti-inflammatory effects of steroidal alkaloids of *Solanum lyratum* Thunb. *Pak. J. Pharm. Sci.,* **37**(2 Suppl.): 463–473.

Yao L, Tian F, Meng Q, Guo L, Ma Z, Hu T, Liang Q and Li Z (2024). Reactive oxygen species-responsive supramolecular deucravacitinib micelles alleviate psoriatic skin inflammation by reducing mitochondrial oxidative stress. *Front. Immunol,* **15**: 1407782.

Yuan LL and Cao CY (2023). Rehmannioside A inhibits TRAF6/MAPK pathway and improves psoriasis by interfering with the interaction of HaCaT cells with IL-17A. *Clin. Cosmet. Investig. Dermatol,* **16**: 2585–2596.

Zhao Y, Gao WK, Wang XD, Zhang LH, Yu HY and Wu HH (2022). Phytochemical and pharmacological studies on Solanum lyratum: A review. *Nat. Prod. Bioprospect,* **12**(1): 39.

Zheng T, Deng J, Wen J, Xiao S, Huang H, Shang J, Zhang L, Chen H, Li J, Wang Y, Ouyang S, Yang M, Otsu K, Liu X and Huang G (2024). p38α deficiency ameliorates psoriasis development by down-regulating STAT3-mediated keratinocyte proliferation and cytokine production. *Commun. Biol.*, **7**: 999.

Zhou P, Feng H, Qin W and Li Q (2023). KRT17 from skin cells with high glucose stimulation promotes keratinocytes proliferation and migration. *Front. Endocrinol. (Lausanne),* **14**: 1237048.

Zhou X, Chen Y, Cui L, Shi Y and Guo C (2022). Advances in the pathogenesis of psoriasis: From keratinocyte perspective. *Cell Death Dis.,* **13**(1): 81.